High-Precision Biomagnetic Measurement System Based on Tunnel Magneto-Resistive Effect

Siming Zuo, Kianoush Nazarpour, Hadi Heidari
Microelectronics Lab (meLAB), James Watt School of Engineering, University of Glasgow, G12 8QQ, UK
School of Inofrmatics, University of Edinburgh, UK
Hadi.Heidari@glasgow.ac.uk

***Abstract*—This paper presents a novel low-noise and high-precision readout circuit for tunnelling magnetoresistive (TMR) array to evaluate the suitability of biomagnetic measurement platform for detection of weak biomagnetic fields. We propose a three operational-amplifier architecture with a high input impedance and an adjustable gain for the fabricated TMR sensor that is highly miniaturized and can be operated at room temperature. The proposed system was designed using standard 0.18 µm CMOS technology and achieved a good performance with regard to gain, linearity, power consumption, and noise by employing a chopper stabilization technique and common mode feedback. The gain can reach 80 dB through adjusting two 5-bit programmable resistors and the input-referred noise voltage only has 44.6 nV/√Hz with 10 nA input bias over a wide range of frequency. Moreover, the whole readout dissipates 58 µW of power with a 1.8 V supply voltage. Benefiting from the CMOS compatibility of the TMR sensor, it offers monolithic integration directly on a silicon substrate as a TMR-on-chip sensing system. This will enable a new scientific and engineering paradigm to revitalize the biomagnetism field as an alternative way to understand the underlying mechanism of the human body.**

Keywords—Analog front-end, Biomagnetic Sensor, Tunnel-Magnetoresistance Effect, Low Noise, Biosignal.

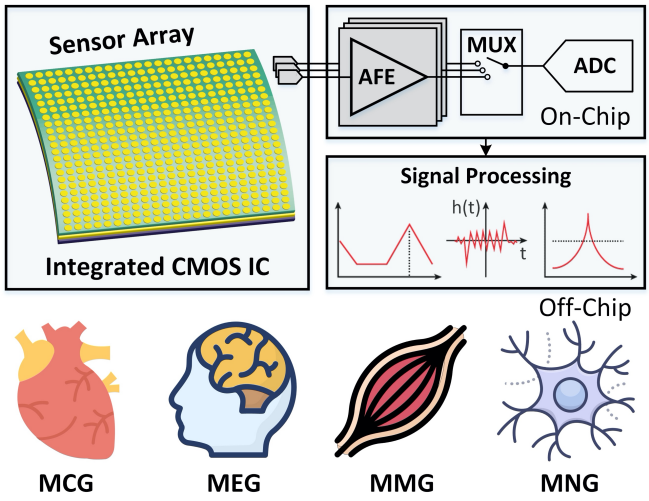

Fig. 1. Block diagram of the proposed biomagnetic sensing system with magnetic sensor array and an integrated CMOS interface including AFE: analog front-end; MUX: multiplexer; ADC: analog-to-digital converter.

I. Introduction

With the rapid progress of micro- and nano-technology, non-invasive assessment of biomagnetism has been a reliable and robust approach and its applications have been extended from clinical diagnoses to human-computer-interaction [1]. Detecting weak biomagnetic fields derived from human active organs and tissues, mainly including Magnetocardiography (MCG) [2], [3], Magnetoencephalography (MEG) [4], [5], Magnetomyography (MMG) [6] and Magnetoneurography (MNG) [7], requires effective methods that offer both high spatial and temporal resolutions. Conventionally, in the clinic, the activity of living tissues is recorded with bioelectricity from the surface of the skin using metal or stainless steel electrodes. However, the electric signals suffer from poor spatial resolution, which is very challenging to target specific tissues, even with high-density needle recording probes. In addition to being painful, the penetration of the needle into the muscle disturbs the muscle structure and function. Moreover, in chronic implants, such as for the motor rehabilitation, the interface between the metal contacts of the sensor and the human tissue changes over time, leading to infection and rejection by the body. Therefore, a different paradigm that enables the recording with a high spatial resolution is needed.

Biomagnetism has become an alternative method and addressed the limitation of the bioelectricity. Firstly, magnetic signals have the same temporal resolution as the electric signal but can offer significantly higher spatial resolution; Secondly, the magnetic approach does not require electric contacts during the recording and therefore, the sensor can be fully encapsulated with biocompatible materials so as to minimise the risk of infection [6]. However, magnetically recording has remained some technical challenges for over four decades. Compared to a high temporal resolution, its spatial resolution is restrained because of some elements such as limited sensor numbers, movement artifacts, intrinsically low signal-to-noise ratio (SNR), and cancellation of background magnetic noise in real-time [8]. Current technologies developed to detect such tiny magnetic field are exploring the use of superconducting quantum interference devices (SQUIDs) [9] and optically-pumped magnetometers (OPMs) [5]. Both experiments are strictly limited in a large magnetically shielded room. These conventional methods are bulky, costly, consume large power and also need a temperature-controlled environment. Herein, the development of highly miniaturized, low-cost, low-power magnetic techniques at room-temperature would revitalize the biomagnetic measurements and constitute an important step toward the wider point-of-use and point-of-care applications for both medical diagnostics and academic research.

Nowadays, spintronic sensors based on a magnetoresistive (MR) effect revolutionise the way magnetic recording owing to their full compatibility with traditional silicon technology. These sensors can be integrated with the readout circuitry onto a standard CMOS process in sub-mm diameter substrates to eventually realize the on-chip signal conditioning, including amplification, filtering, noise and drift cancellation [10]. This phenomenon has led to the development of the MR sensors with ultra-high sensitivity, which have gradually replaced the traditional thin-film magneto-transport devices such as Hall sensors [11] and have the potential to detect pico-Tesla range magnetic fields, appropriate for biomagnetic signal level. In addition, the miniaturized MR sensor area can improve the resolution of fields with small distance changes. The sensor placed at a closer distance to the neural sources will provide stronger signals. The MR sensors, thereby, are suitable for array applications with a lower power requirement. Recently, giant magnetoresistive (GMR) sensors were used to record weak biomagnetic signals. However, the sensitivity of GMR sensors is in the nano-Tesla range and therefore averaging was required to enhance the SNR. Over the last decade, sensing at pico-Tesla/√Hz level fields has become possible with the tunnelling magnetoresistive (TMR) sensors that are highly miniaturized and can be operated at room temperature using a sensor array with a large number of sensors.

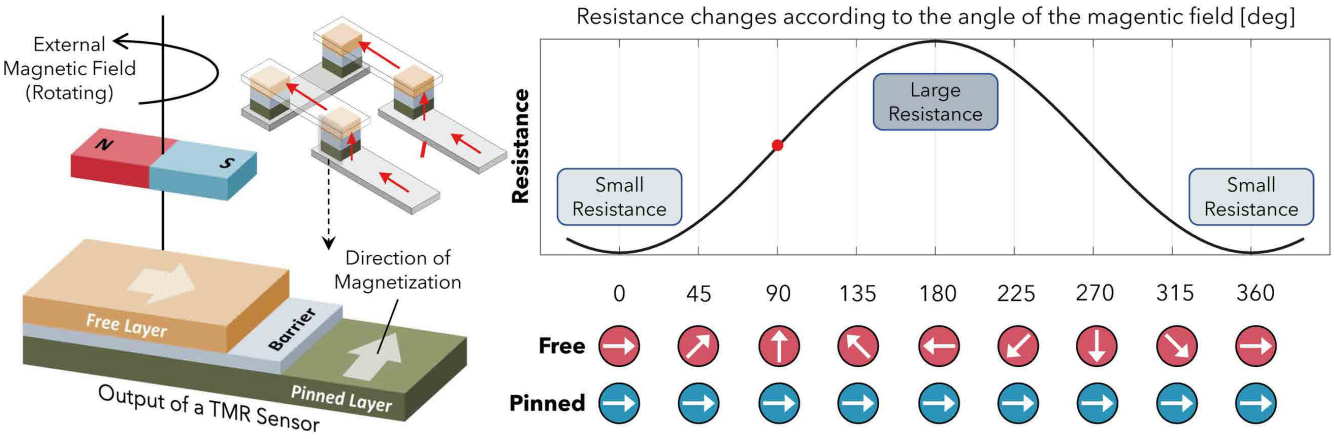

Fig. 2. Schematic diagrams of a TMR sensor typical structure and its transfer curve with resistance changes according to the angle of the magnetic field.

Integrated electronics that use instrumentation systems have been expanded from the initial signal amplification only to the subsequent conditioning, data conversion and signal processing. In the integrated detection system. Figure 1 shows our proposed real-time measurement system including a large array of TMR sensors and an on-chip analog front-end that has parallel or multiplexed analog outputs. This paper describes the design of a low noise readout integrated circuit with chopper-stabilized three operational amplifiers suitable for a Wheatstone bridge configuration of TMR sensors.

II. Architecture Overview

A. TMR Sensor Design

Spintronics is the study of a fundamental property of electrons known as their spin. Some materials exhibit spin-related magnetoresistive properties at room temperature that results in a change of their electrical resistance when exposed to an external magnetic field. Tunnelling is a nanoscale effect where electrons can pass through a very thin (sub-nanometre) insulating material under the right condition, exhibiting spin-related magnetoresistive properties at room temperature. That is called tunnelling magnetoresistance (TMR). The typical structure and its transfer curve are shown in Fig. 2. The TMR sensor comprises two layers of ferromagnetic (FM) material separated by an insulation layer. The top layer is defined as a free layer since its magnetization direction can be changed freely, and the bottom layer is called a pined layer due to its fixed magnetization orientation when the sensor is fabricated. The probability of electrons that are quantum-mechanically tunnelling across an insulator depends on the orientation of two FM layers. To indicate the maximum signal that can be obtained from the sensor, the TMR ratio as a figure of merit for the sensor traditionally can be defined as:

$$TMR(\%) = \frac{R_{max} - R_{min}}{R_{min}} \times 100 \qquad (1)$$

where R_{max} and R_{min} are the largest and lowest values of the resistance in Ohms when the magnetizations of two FM layers are in antiparallel and parallel alignments.

For biomagnetic measurement, the TMR response has to be linear with hysteresis-free, being able to detect ultralow magnetic fields. The details of linearization strategies for high sensitivity MR sensor are demonstrated in [12]. The sensor sensitivity can be calculated from a slope of the experimental transfer curve and represent how much the sensor responds to field changes, while the noise level will determine the limit of detection. According to theoretical calculation and experiment outcomes, the best overall noise performance is obtained with large arrays of large area sensors [13]. Therefore, 1102 TMR sensors are connected as 38 rows and 29 columns in series to minimize sensor 1/*f* noise. Each TMR element comprises of (unit: nm) [5 Ta / 25 CuN] × 6 / 5 Ta / 5 Ru / 20 IrMn / 2 $CoFe_{30}$ / 0.85 Ru / 2.6 $CoFe_{40}B_{20}$ / MgO [9 kΩ·μm^2] / 2 $CoFe_{40}B_{20}$ / 0.21 Ta / 4 NiFe / 0.20 Ru / 6 IrMn / 2 Ru / 5 Ta / 10 Ru. Figure 3 shows the actual sensor array image under a microscope. The size of each TMR element is 100 × 100 μm and electrode pads (200 × 400 μm) are separated by 250 μm.

A Wheatstone bridge structure is employed to minimize the temperature drift and also to nullify the output signal in the absence of any applied magnetic field. Combining four TMR sensor arrays in a full Wheatstone bridge configuration will enable us to increase magnetic field detectivity and electrical robustness, reduce power consumption and achieve better sensitivities so as to obtain competitive results. Setting a bias current of 20 mA, the measured linear range is approximately −1 Oe to 1 Oe. The average $R \times A$ is 9 kΩ·μm^2 with uniformity of 13% over all the wafer and the TMR ratio is 152% with uniformity of 9%. As the full bridge setup, the measured resistance variation of each TMR sensor is 280 Ω·μm^2/Oe. Thus, for 1102 elements with the area of 100 × 100 μm^2, the sensitivity is calculated as ~ 0.617 V/Oe.

B. Readout Circuit Design

The complete signal processing chain is demonstrated in Fig. 4(a), which comprises a full Wheatstone bridge circuit, input buffers, a differential amplifier, a low pass filter (LPF)

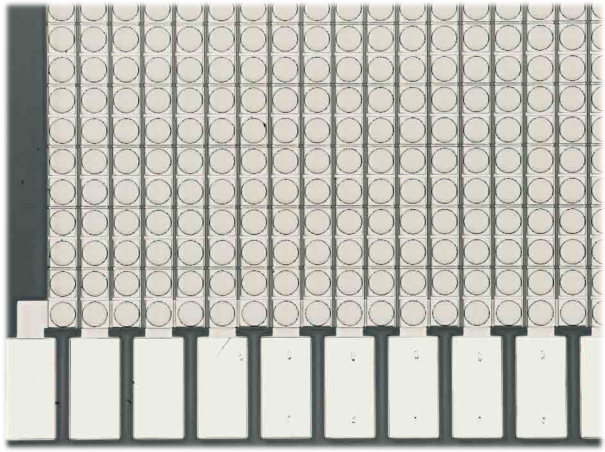

Fig. 3. A microscope image of the TMR sensor array.

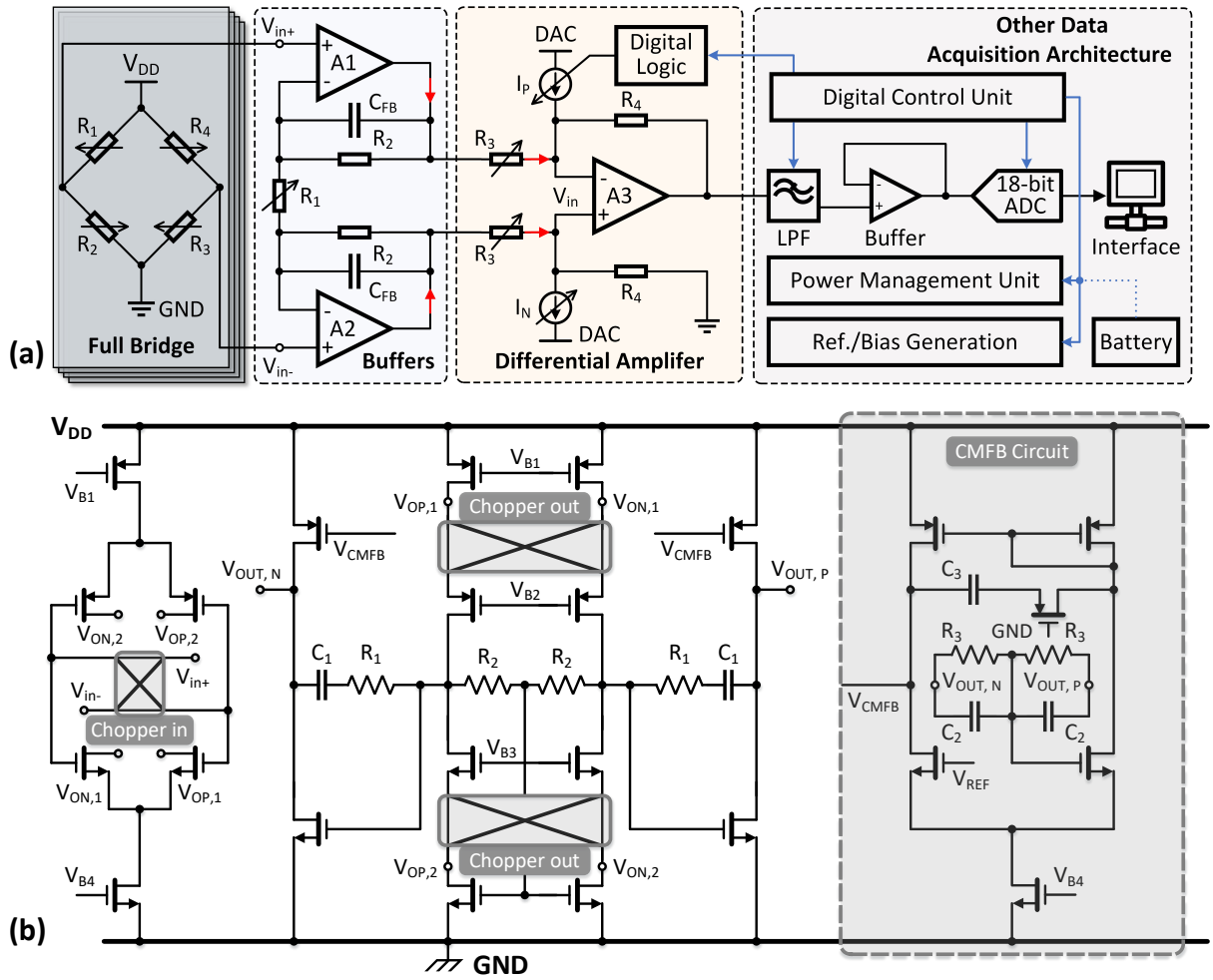

Fig. 4. (a) A processing chain of the proposed biomagnetic sensing systems; (b) Schematic of the readout IC with the chopper-stabilized technique.

and a microcontroller unit with an analog-to-digital converter (ADC) and SPI interface. In this work, we proposed a three-operational amplifier architecture with the use of two low-noise input amplifiers as a first stage, consisting of A_1 and A_2, and a second stage, A_3, ultimately to achieve a high input impedance, excellent linearity and extend the input range by using rail-to-rail input stages. Additionally, a comfortably adjustable gain of each stage is achieved by variable resistors, R_1 and R_3, connected to a 5-bit digital-to-analog converter (DAC) as 5-bit programmable resistors. The transfer function of the proposed three-operational amplifier structure including the DAC operation is expressed as

$$V_{out} = \left(1 + \frac{2R_2}{R_1}\right)\left(\frac{R_4}{R_3}\right)(V_{in+} - V_{in-}) + R_4(I_P + I_N) \quad (2)$$

The two single-ended amplifiers A_1/A_2 as input buffers generate low noise through a chopper stabilization technique, chopping the frequency to eliminate upmodulating offset and low-frequency flicker noise [14], while the fully differential amplifier, A_3, is used at a folded cascode stage as a chopping output. Figure 4(b) illustrates the schematic of the proposed amplifier structure. The total noise is a combination of input stage noise and output stage noise, which are the square root of the sum of the noise sources, defined as

$$V_{ni,Total} = \sqrt{(e_n)^2 + (R_S \times i_n)^2 + V_n(R_{EX})^2} \quad (3)$$

where $V_{ni,\,Total}$ is the total noise referred-to-input; e_n is input-referred voltage noise; i_n is input-referred current noise; R_S is an equivalent input resistance to the amplifier; $V_n(R_{EX})$ is voltage noise from external circuitry. It is thus significantly important to push the input-referred voltage noise down to sub-nV/√Hz and the input-referred current noise down to sub-pA/√Hz at a wide range of frequencies.

Furthermore, the common-mode feedback (CMFB) circuit is employed to maintain DC voltage outcomes [15]. It detects the common-mode voltage, compares with a reference, and return the compared result to the bias network. Fixing the DC output at the required level, it finally eliminates the output common-mode current component. After the chopper- and CMFB-stabilized pathway, the amplified signal is then passed through a high-order (20th), adopting a Sallen-key topology with a cutoff frequency from 300 to 500 Hz, appropriate for biomagnetic signals [1]. Subsequently, the filtered signals are converted into digital data through an 18-bit successive approximation register ADC that offers high speed, high accuracy, low-power and low-cost. Eventually, the signals are transferred via a wireless module and identified, characterized and quantified with a LabVIEW interface on the laptop.

The readout circuit design was designed and simulated in a standard CMOS 0.18 μm technology to achieve acceptable performance, in terms of linearity, offset and noise, before fabricating the chip. The Wheatstone bridge was modelled by COMSOL based on a finite-element method and then the parameter of variable resistance was defined using Verilog-A language. The ultimate goal is to address the challenges of monolithic integration of the TMR sensor array directly on a silicon substrate as a TMR-on-chip sensing system.

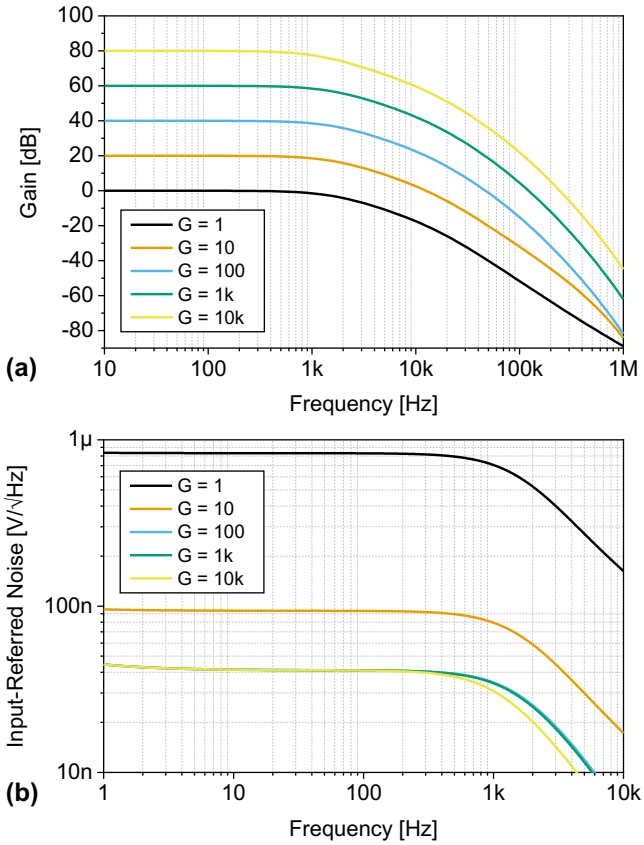

Fig. 5. Simulated transfer functions: (a) gain; (b) input-referred noise.

III. Simulation Results

The gain and noise performance of the simulated readout IC is shown in Fig. 5. The input impedance is extremely high and approximately 10^9 Ω. This input bias current is very low at about 10 nA, which ensures very little changes with varying input voltage. The differential mode gain of the proposed readout circuit is illustrated in Fig. 5(a). With a supply voltage of 1.8 V, the DC gain and the bandwidth are 80 dB and 1 kHz with a phase margin of 62.5 degree. The gain accuracy and the ability to suppress common-mode signals are improved. The common-mode rejection ratio can reach 108 dB to minimize the noise from strong electromagnetic interference. Table I summaries and compares the simulated AFE performance. Although the bandwidth is not as high as that of other works, it is high enough to amplify weak low-frequency biomagnetic signals. The input-referred voltage noise versus frequency is shown in Fig. 5(b). The AFE achieves a noise performance of 44.6 nV/√Hz with low-pass filtering at a cutoff frequency of 1 kHz, which makes it appropriate for the high-resolution and low-noise biosignal recording. The noise is increased at the low-frequency domain due to the 1/*f* noise, which affects performance in gains less than 10. Finally, from the filtering simulation, filters with a lower cutoff frequency will produce the minimum noise for the high-precision measurements.

IV. Conclusion

In summary, we develop a low-noise and high-precision three-operational amplifier architecture readout IC for TMR sensors with a chopper stabilization and CMFB technique. The proposed readout circuitry is designed and simulated in a standard 0.18 µm CMOS. The simulation results show that it realizes good performances in respect of gain, linearity, power consumption, and noise level to record biomagnetic signals. It dissipates 58 µW of power using a 1.8 V supply voltage. The amplifier employs a gain of 20 to 80 dB using two 5-bit programmable resistors. Benefiting from the ultralow input-referred voltage density of 44.6 nV/√Hz over the 1 to 1 kHz range with only 10 nA input bias current, the proposed system would enable significant advances towards high temporal and spatial resolution measurements to identify, characterize and quantify the biomagnetic signals in the future.

Table I: Comparison table with state-of-the-art works.

Parameter	2011 [16]	2013 [17]	2019 [18]	This Work
Technology	0.5 µm	0.18 µm	0.18 µm	0.18 µm
Supply (V)	1.8	1.8	1.8	1.8
Gain (dB)	45	67.7	40.48	80
CMRR (dB)	75	92	114.2	108
Phase Margin	N/A	N/A	N/A	62.5°
Offset Voltage	N/A	N/A	N/A	120 µV
Bandwidth (Hz)	1.1M	1.1M	1M	1k
Input Noise (V/√Hz)	~22n	89n	N/A	44.6n
Power Diss. (µW)	~ 280	263	27	58

References

[1] J. Malmivuo and R. Plonsey, *Bioelectromagnetism: principles and applications of bioelectric and biomagnetic fields*. Oxford University Press, USA, 1995.

[2] D. B. Geselowitz, 'Magnetocardiography: an overview', *IEEE Trans. Biomed. Eng.*, no. 9, pp. 497–504, 1979.

[3] R. Fenici, D. Brisinda, and A. M. Meloni, 'Clinical application of magnetocardiography', *Expert Rev. Mol. Diagn.*, vol. 5, no. 3, pp. 291–313, 2005.

[4] S. Baillet, 'Magnetoencephalography for brain electrophysiology and imaging', *Nat. Neurosci.*, vol. 20, no. 3, pp. 327–339, 2017.

[5] E. Boto *et al.*, 'Moving magnetoencephalography towards real-world applications with a wearable system', *Nature*, vol. 555, no. 7698, p. 657, 2018.

[6] S. Zuo, H. Heidari, D. Farina, and K. Nazarpour, 'Miniaturized magnetic sensors for implantable magnetomyography', *Adv. Mater. Technol.*, 2020.

[7] B.-M. Mackert, 'Magnetoneurography: theory and application to peripheral nerve disorders', *Clin. Neurophysiol.*, vol. 115, no. 12, pp. 2667–2676, 2004.

[8] C.-H. Im, S. C. Jun, and K. Sekihara, 'Recent advances in biomagnetism and its applications'. Springer, 2017.

[9] R. Kleiner, D. Koelle, F. Ludwig, and J. Clarke, 'Superconducting quantum interference devices: State of the art and applications', *Proc. IEEE*, vol. 92, no. 10, pp. 1534–1548, 2004.

[10] S. Zuo, K. Nazarpour, and H. Heidari, 'Device modelling of MgO-barrier tunnelling magnetoresistors for hybrid spintronic-CMOS', *IEEE Electron Device Lett.*, 2018.

[11] H. Heidari, S. Zuo, A. Krasoulis, and K. Nazarpour, 'CMOS Magnetic Sensors for Wearable Magnetomyography', in *40th Inter. Conf. of the IEEE Engineering in Medicine and Biology Society*, 2018.

[12] A. V Silva, D. C. Leitao, J. Valadeiro, J. Amaral, P. P. Freitas, and S. Cardoso, 'Linearization strategies for high sensitivity magnetoresistive sensors', *Eur. Phys. J. Appl. Phys.*, vol. 72, no. 1, p. 10601, 2015.

[13] S. Zuo, K. Nazarpour, T. Böhnert, R. Ferreira, and H. Heidari, 'Integrated Pico-Tesla Resolution Magnetoresistive Sensors for Miniaturised Magnetomyography', in *42th Annual Inter. Conf. of the IEEE Engineering in Medicine and Biology Society*, 2020.

[14] J. F. Witte, K. A. A. Makinwa, and J. H. Huijsing, 'A CMOS Chopper Offset-Stabilized Opamp', *IEEE J. Solid-State Circuits*, vol. 42, no. 7, pp. 1529–1535, 2007.

[15] S. Zuo, H. Fan, K. Nazarpour, and H. Heidari, 'A CMOS Analog Front-End for Tunnelling Magnetoresistive Spintronic Sensing Systems', in *IEEE International Symposium on Circuits and Systems (ISCAS)*, 2019.

[16] M. Goswami and S. Khanna, 'DC suppressed high gain active CMOS instrumentation amplifier for biomedical application', in *2011 International Conference on Emerging Trends in Electrical and Computer Technology*, 2011, pp. 747–751.

[17] A. Goel and G. Singh, 'Novel high gain low noise CMOS instrumentation amplifier for biomedical applications', in *Inter. Conf. on Machine Intelligence and Research Advancement*, 2013.

[18] M. Konar, R. Sahu, and S. Kundu, 'Improvement of the Gain Accuracy of the Instrumentation Amplifier Using a Very High Gain Operational Amplifier', in *2019 Devices for Integrated Circuit (DevIC)*, 2019.